ELSEVIER

International Journal of Mass Spectrometry 190/191 (1999) 37–45

International Journal of Mass Spectrometry

Kinetic energy of an N^+ ion cloud throughout the stability diagram

M. Vedel*, J. Rocher, M. Knoop, F. Vedel

Physique des Interactions Ioniques et Moléculaires, UMR 6633 CNRS-UAM1, Université de Provence, Centre de St-Jérôme, Case C21, F13397 Marseille Cedex 20, France

Received 2 November 1998; accepted 31 December 1998

Abstract

A precise time-of-flight method previously developed is used to investigate the average kinetic energy of an N^+ ion cloud. From values obtained for different points in the Mathieu stability diagram, variation of the kinetic energy versus the corresponding experimental parameters is estimated. It is observed that the magnitude depends essentially on the smallest two-dimensional component of the three-dimensional potential well. Measurements at different radiofrequencies (0.5, 1, and 1.5 MHz) show that the kinetic energy does not increase with the rf frequency. From the observed temporal variation of the kinetic energy, collisional cooling is evidenced. (Int J Mass Spectrom 190/191 (1999) 37–45) © 1999 Elsevier Science B.V.

Keywords: Paul trap; Kinetic energy measurements; Time-of-flight methods

1. Introduction

Ion storage in a Paul trap can be used for a large variety of applications [1,2]. Precise knowledge of the kinetic energy of the ions stored in a rf trap is generally important information, even if it is not imperative, as for instance, when preparing ions for ion/molecule collisions. Although the term "kinetic energy" of an ion cloud is ambiguous, it is of widespread use. In this article we will apply the definition generally given in the literature [3]. See [4]. The term kinetic energy designates the rf-averaged value of the sum of the statistical averages of each component of the ion motion. Most of the time these components can be considered to follow Gaussian distributions. In the absence of space charge, spatial and velocity distributions of each component are related by the equations of motion and then only two parameters are needed to describe the entire statistical properties of the ion cloud, which fortunately limits the number of experiments [4]. The most precise and rapid method to determine the kinetic energy of the trapped ions consists of measuring their velocity distribution from the Doppler profile of a fluorescence line, which also allows us to check the Gaussian character of the distribution [5]. Moreover, it does not alter the ion storage properties. This method is, however, only possible for ions presenting an accessible optical transition and requires the use of a tunable laser. Other nondestructive methods, electronic instead of optic, as noise resistor measurements [6] cannot be easily applied in Paul traps due to the

* Corresponding author. E-mail: fern@frmrs12.u_3mrs.fr

Dedicated to J.F.J. Todd and R.E. March in recognition of their original contributions to quadrupole ion trap mass spectrometry.

PII S1387-3806(99)00004-4

presence of the rf frequency because they are actually limited to very light particles and to Penning traps. In summary, time-of-flight (TOF) methods appear to be the most universal and flexible [7–9]. We have presented such a method [10] and its improvement by choosing a specific ejection phase [7]. This technique has been validated in comparison with the chemical thermometer method [11]. It is well adapted to our ion detection technique (which is based on the ejection of ions by interruption of the trapping voltage) [12].

The modelling and energy calibration of the time-of-flight profile requires that the rf field be interrupted as close to zero as possible, without parasitic oscillations. In a recent article [13] we have described specific electronics in order to open the method to higher rf frequencies. By modelling the unavoidable residual voltage at the instant of the rf interruption in any situation, the method can now be matched to many working conditions.

In this article, we will first describe the experimental setup in Sec. 2.1. In Sec. 2.2, we report results, where we apply the TOF method to investigate the kinetic energy of an N^+ ion cloud in the presence of the neutral N_2 gas as a function of the potential well depth for different working points of the stability diagram. The temporal evolution of the kinetic energy will also be presented. Finally, conclusions and an outlook will be given.

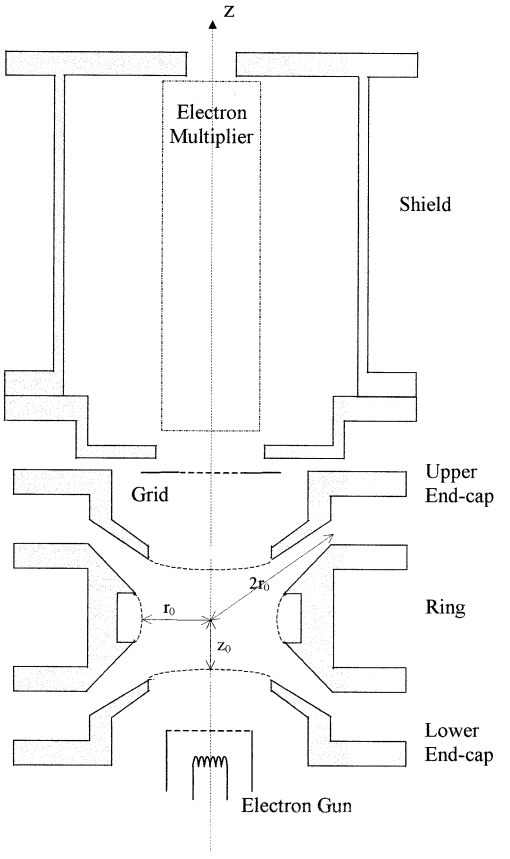

Fig. 1. Experimental setup.

2. Method

2.1. Experimental

The setup (Fig. 1) is the same as described in [13]. The ion trap made from stainless steel is formed by three hyperbolic electrodes. The ring electrode (r_0 = 14 mm) has a total height of 30 mm. The two endcap electrodes, $2z_0$ = 20 mm apart and 35 mm in width, have their central region (25 mm) replaced with mesh to allow the escape of electrons and ions (during the gas ionisation and the detection). A potential $V(t)$, $[V(t) = V_{ac} \cos \Omega t + U_{dc}]$, is applied to the ring electrode, while the two endcaps are grounded. The trap is mounted in a 2.5 L ultrahigh vacuum (UHV) chamber equipped with a microvalve allowing introduction of pure nitrogen gas. The residual pressure is below 1×10^{-9} mbar. During measurements the nitrogen pressure is maintained at 2×10^{-8} mbar by an ion and a turbomolecular pump, monitored with a mass spectrometer (Balzers QMG 64) and a Bayard–Alpert gauge (Granville-Philips 274).

The work presented here has been done with an N^+ ion cloud created inside the trap by 150 eV electron impact dissociation of neutral N_2. The ion creation time is fixed at 150 ms. It is assumed that about 90% of the created ions are N_2^+, 10% are N^+, and a very small amount consist of N_2^{++}. The working point is chosen in a such way that the major component N_2^+ has no stable trajectories and only ions with a mass-to-charge ratio equal to 14 are stored. N_2^{++} ions react quickly and are eliminated almost instantaneously.

After creation, ions driven by the rf field are trapped for times of 50 ms to a few seconds. At the end of the storage time ($t = t_0$), the alternating voltage (applied to the ring) is interrupted at a rf phase ϕ_C corresponding to $V(t) = 0$ ($\phi_C = \Omega t_0 = \pi/2 + 2k\pi$). For technical reasons, the cutoff of the voltage cannot be perfect and a small but unavoidable overshoot is still present after t_0. Then, inside the trap, ions are subjected to the potential Φ which is given by:

$$\Phi(x, y, z, t_0 < t < t_c) = \frac{V_{\text{tot}}}{2r_0^2}(x^2 + y^2 - 2z^2) + \frac{V_{\text{tot}}}{2}$$

where: t_c corresponds to the instant at which the ion i reaches the upper endcap electrode, V_{tot} is the total voltage present on the ring electrode after t_0, it is the sum of the dc component of the storage voltage (U_{dc}) and the small overshoot (V_{res}) after interruption of the radiofrequency [7,13].

To detect ions escaping from the trap, we use an electron multiplier (EM). It is situated along the trap z axis, at 28 mm above the upper endcap. The first dynode has a rectangular opening (12 mm × 7 mm) and needs a polarisation high voltage between −2000 and −1000 V. In order to protect ions from the high voltage during their crossing of the equipotential region, a grounded grid of 12 mm diameter is fixed at a distance of 8 mm in front of the EM. Ions are then moving in a field-free region between the grounded upper endcap and the protective grid and they are greatly accelerated beyond this grid. This allows us to determine an unperturbed TOF profile. The current delivered by the EM is amplified by a charge amplifier. The signal is then directly visualised by a digital oscilloscope (Tektronix 2221A) triggered at $t = t_0$. A TOF profile is obtained. It gives the necessary information for the determination of the average kinetic energy of the ion cloud at the instant of the interruption of the confinement voltage.

Measuring the ion kinetic energy implies the preparation and storage of a pure N^+ ion cloud. To be free from parasitic species, we can create a cloud at working point $(a_z; q_z)_{\text{crea}}$, where only N^+ ions have stable trajectories and confine it at the same point or transport it to any other point (corresponding to the "measurement point") with the same q_z value by only changing the U_{dc} voltage applied to the ring electrode. In this way, the whole stability diagram is accessible.

Measurement of energy requires stable conditions of storage. Indeed, if the chosen working point corresponds to a condition for nonlinear resonances [14–16], the simulation based on the hypothesis of a quadrupole trapping field cannot be used anymore and modifications of the cloud become difficult to control: spatial and velocity distributions are no longer Gaussian, part of the ions are lost and storage times decrease rapidly. As a consequence, we controlled our position in a proper zone of the stability diagram by measuring the frequency spectrum of the ion motion [14,16].

2.2. Time-of-flight method

As has already been described in a previous article [13] the experimental profiles are compared to TOF curves obtained by a three-dimensional simulation modelling the progress of about 10^6 ions in our system (from the instant of their creation in the trap to their impact on the first dynode of the EM). The simulation is based on the hypothesis that both spatial and velocity distributions are Gaussian. In order to keep this property during the simulation, it is verified that the extensions of the distributions are much smaller than the system dimensions. The confinement potential is taken to be purely quadrupolar. From the measurement of the frequency spectrum of ion motion, it has been deduced that space charge effects are sufficiently weak to be neglected. Moreover, we have verified that the expected variation [4] of the secular frequencies in the simulation due to ion–ion collisions did not result in a kinetic energy modification at the present ion density. Furthermore, collisions between ions and neutrals are not taken into account by the simulation.

Standard deviations of the initial distributions at a phase equal to zero (or $t = 0$) corresponding to a given value of the average ion kinetic energy and of the anisotropy coefficient $\mathbf{c_A}$ (the ratio between the axial and corresponding radial dispersions [4]) are determined for each working point. The parameters a

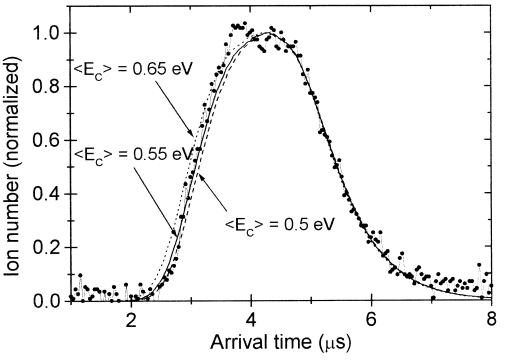

Fig. 2. Adjustment of an experimental profile (dots) obtained for $V_{ac} = 110\ V_{rms}$, $U_{dc} = 19$ V, $\Omega/2\pi = 1$ MHz ($q_z = 0.543$; $a_z = -0.132$) with three profiles calculated with $E_{lab} = 0.5$, 0.55, 0.65 eV and $c_A = 1$ (from [13]).

and q are evaluated from the secular frequencies (ω_z and ω_x) deduced from the measured ion motion spectrum [12] where $\omega_u = \beta_u(\Omega/2)$, with $u = r, z$. In the so-called adiabatic approximation [3], β_u can be expressed as $\beta_u = \sqrt{a_u + (q_u^2/2)}$. Ionic samples with given initial position and velocity distributions can then be generated according to the assumed distributions. A simulated histogram of ion number reaching the EM in 500 successive intervals at a time of 0.04 μs is constructed via calculations of 3D ion trajectories along the different parts of the setup. To accurately reproduce the progress of the ions, these calculations take into account the geometry of the apparatus and the voltages applied to the electrodes and grids during a measurement sequence cycle. In particular, the total residual voltage present on the ring electrode after the storage voltage cutoff is precisely modelled. When the applied radio frequency is equal to 0.5 or 1 MHz, V_{res} can be approximated by a constant and the calculations of ion trajectories are carried out easily by using the analytical solutions of the differential equations. In the case of 1.5 MHz storage frequency, the time dependence of V_{res} cannot be neglected and the resolution of the equations of motion is carried out with a fourth-order Runge–Kutta algorithm. Histograms are compared with experimental profiles and kinetic energy and anisotropy coefficients are determined from the best fit [13], an example of which is given in Fig. 2.

In this article, the working points were characterised by a total potential well depth called $\mathcal{D}_{tot}$ (defined as $\mathcal{D}_{tot} = \mathcal{D}_r + \mathcal{D}_z$), with $\mathcal{D}_r = \frac{1}{2}m\omega_r^2 r_0^2$ and $\mathcal{D}_z = \frac{1}{2}m\omega_z^2 z_0^2$) or by the couple ($\mathcal{D}_r$, $\mathcal{D}_z$), where the motional frequencies ω_r and ω_z are deduced from the systematically measured spectra of ion motion. Using the adiabatic approximation the potential well depth can also be written in the following way:

$$\mathcal{D}_r = \frac{mr_0^2}{8}\left(a_r + \frac{q_r^2}{2}\right)\Omega^2$$

and

$$\mathcal{D}_z = \frac{mz_0^2}{8}\left(a_z + \frac{q_z^2}{2}\right)\Omega^2$$

We evaluate the average kinetic energy by changing the well depth: $\mathcal{D}_z$ in a range up to 17 eV, and $\mathcal{D}_r$ up to 11 eV; $\mathcal{D}_{tot}$ increases proportionally to q_z. At a fixed value of $\mathcal{D}_{tot}$, $\mathcal{D}_z$, and $\mathcal{D}_r$ can be varied by changing a_z, or $\mathcal{D}_{tot}$ can be increased for the same q_z range by choosing a higher radiofrequency ($\Omega/2\pi$).

3. Results

Preliminary studies have been carried out at a radiofrequency $\Omega/2\pi$ of 500 kHz for a potential depth of 4 eV. By increasing $\Omega/2\pi$ and the amplitude of the storage voltage, it is possible to obtain a deeper potential well depth ($\mathcal{D}_{tot}$) for the same q_z value. Here, we will present the results of our evaluation of the average kinetic energy through the stability diagram. We have carried out two further campaigns of measurements at 1 and 1.5 MHz. We have also measured the temporal variation of the kinetic energy for the trapped ions.

3.1. Measurements at $\Omega/2\pi = 1$ MHz

Experimental profiles have been realised with a large range of working points. The confinement voltages were varied in the following ranges: $80\ V_{rms} < V_{ac} < 122\ V_{rms}$; $3\ V < U_{dc} < 20$ V (that is to say: $0.40 < q_z < 0.60$ and $-0.14 < a_z < -0.02$). The corresponding variation of the potential well depth lies between 0.85 and 11 eV for $\mathcal{D}_z$ and between 6.9 and 16.9 eV for $\mathcal{D}_r$. The larger values for $\mathcal{D}_z$ with

respect to $\mathcal{D}_r$ are due to the fact that we chose working points for which only N^+ species have stable trajectories. For this trapping frequency, the residual voltage (V_{res}), present on the ring when the rf voltage is interrupted, is constant and equal to only a few volts. In order to adjust the experimental profiles in the best way, the value of the anisotropy factor $\mathbf{c_A}$ was generally taken close to 1. The average kinetic energy of the ions (in the laboratory frame) was varied between 0.55 and 2.45 eV with an absolute uncertainty of 0.1 eV (giving relative uncertainties of 18–4%).

3.2. Measurements at $\Omega/2\pi = 1.5$ MHz

The measurements at 1.5 MHz have been realised with V_{ac} varying from 163.5 to 258 V_{rms} and U_{dc} chosen between 15 and 43 V, corresponding to $0.36 < q_z < 0.56$ and $-0.132 < a_z < -0.046$ (1.31 eV $< \mathcal{D}_z <$ 20.75, 14.4 eV $< \mathcal{D}_r <$ 34.8 eV). Because of the presence of oscillating overshoots at the rf voltage interruption, the residual voltage is now time-dependent and on the order of 10 V. To adjust the experimental profiles we had to use a larger range for the anisotropy factor ($0.6 < \mathbf{c_A} < 1$). This could stem from the more important discrepancy between $\mathcal{D}_r$ and $\mathcal{D}_z$. Larger relative uncertainties on the energy evaluation were obtained (between 40 and 10%). The evaluated kinetic energy varied from 0.3 to 2.5 eV in the laboratory frame.

3.3. Discussion

The energy measurements versus the total potential well depth and for the different rf frequencies values are reported in Fig. 3. All the points have been labelled, and identical letters are given for points with identical q_z values. In the following figures the same letters for the same working points have been used. From the repartition of the points, we observe that—even for the higher radiofrequency and at deeper potential well depths—the kinetic energy versus the potential depth is limited to about 2.5 eV. A more regular variation can be obtained when only one parameter is varied. Measurements made at a constant

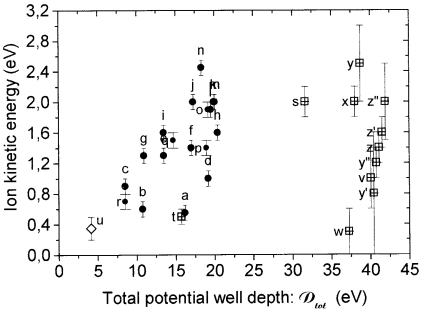

Fig. 3. Ion kinetic energy as a function of the total potential well depth ◇: 500 kHz; ●: 1 MHz; ⊞: 1.5 MHz. All the points have been labelled, identical letters are given for points with identical q_z values. In the following figures the same letters for the same working points have been used.

q_z value at $\Omega/2\pi = 1.5$ MHz showed that the kinetic energy increases linearly with $\mathcal{D}_z$ (see Fig. 4). In this case we found the relation between the kinetic energy (KE) and the axial potential well depth to be: KE = (0.096 ± 0.002) $\mathcal{D}_z$ (where the kinetic energy is expressed in eV). This law is similar to previous measurements [17,18]. Actually, the fitted slope can be very different for other cases. For instance, for $\Omega/2\pi = 1$ MHz and $-0.13 < a_z < -0.02$ and $q_z = 0.588$ we found: KE = (0.037 ± 0.002) $\mathcal{D}_z$.

Because our experimental conditions almost always correspond to $\mathcal{D}_z$ smaller than $\mathcal{D}_r$, it will be this first value that will induce the variation of the kinetic energy (Fig. 5). Indeed, it is the smallest potential,

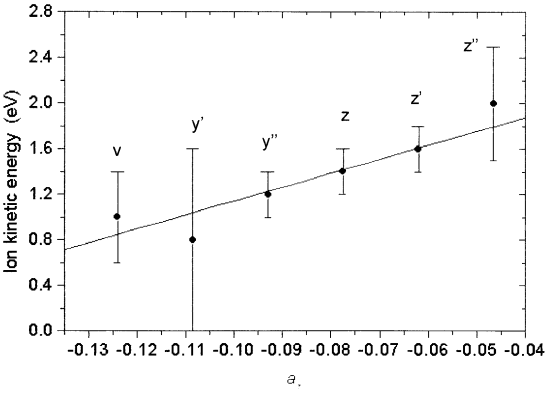

Fig. 4. Ion kinetic energy as a function of a_z at $q_z = 0.57$. Trapping frequency $\Omega/2\pi = 1.5$ MHz.

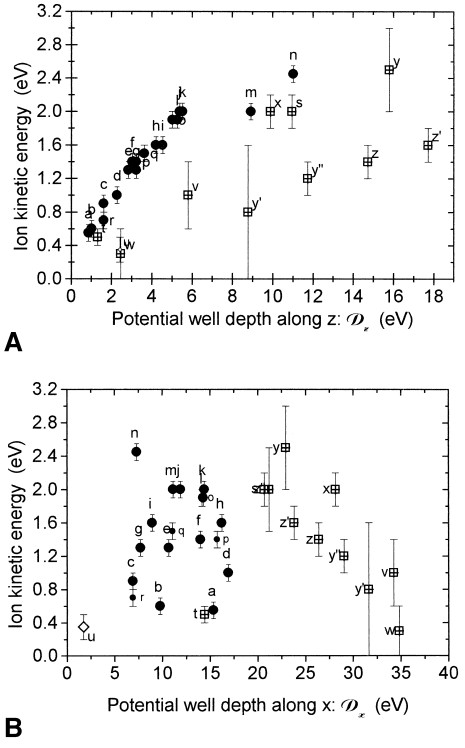

Fig. 5. Ion kinetic energy as a function of $\mathcal{D}_z$ (a) and $\mathcal{D}_r$ (b); ◇: 500 kHz; ●: 1 MHz; ⊞: 1.5 MHz.

min($\mathcal{D}_r$, $\mathcal{D}_z$), which limits the total kinetic energy, since the evaporative cooling is governed by this threshold. This fact was already noticed in [19]. However, the energy increases when the ratio $\mathcal{D}_z/\mathcal{D}_r$ tends to 1 (Fig. 6). For the same value of the ratio (but for different values of $\mathcal{D}_z$ and $\mathcal{D}_r$) the dispersion of

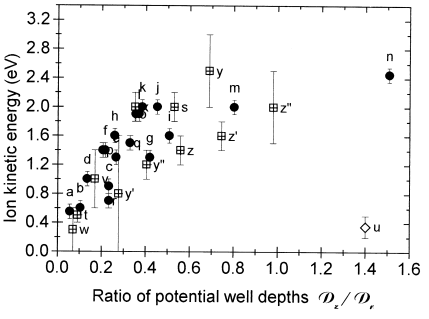

Fig. 6. Ion kinetic energy versus $\mathcal{R} = \mathcal{D}_z/\mathcal{D}_r$, ◇: 500 kHz; ●: 1 MHz; ⊞: 1.5 MHz.

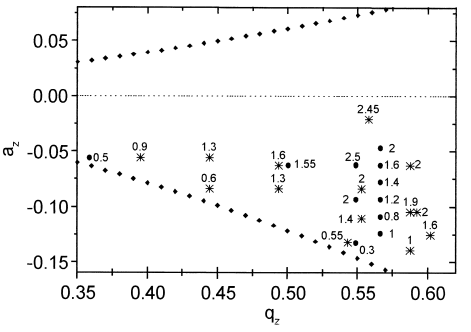

Fig. 7. Various measurements of the kinetic energy of the N^+ ions in the stability diagram, * $\Omega/2\pi$ = 1 MHz, ●: $\Omega/2\pi$ = 1.5 MHz.

the points shows that the kinetic energy is higher when the total potential is bigger.

The described measurements of the kinetic energy can also be represented in the stability diagram (Fig. 7). This presentation shows that inside the investigated region, the isoenergy lines close to the $\beta_r = 0$ border follow iso-β_r lines and that the maximum for the energy is situated at about $q_z = 0.55$ and $a_z = -0.06$. This value is remarkably close to the value found in [5] from fluorescence measurements ($q_z = 0.55 \pm 15\%$ and $a_z = -0.03 \pm 10\%$).

3.4. Effects of the trapping duration on the time-of-flight profile

The first example reported here concerns an ion cloud created during a 150-ms ionisation period and confined at $V_{ac} = 118\ V_{rms}$, $U_{dc} = 15$ V, $\Omega/2\pi = 1$ MHz ($a_z = -0.104$; $q_z = 0.582$) at a neutral nitrogen pressure of 2.8×10^{-8} mbar. While increasing the storage duration of the created ions from 400 ms to 14 s (Fig. 8) we observe a decrease of the detected ion number, as well as a reduction of the profile width with a shift of the rising edge of the profile to longer times. This latter effect can be explained by a cooling mechanism of the cloud. This hypothesis is however insufficient to reproduce the exact evolution of the profile, since the effects of elastic and inelastic collisions are not taken into account in the simulation; nevertheless it allows us to adjust the width and the shift of the profile in a very satisfactory way (see Fig.

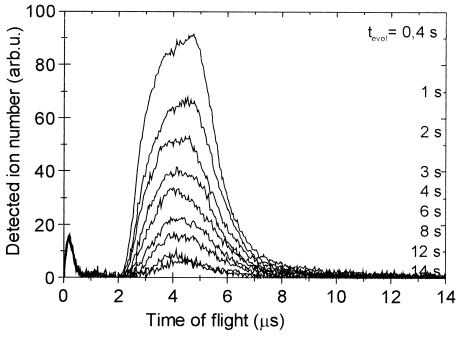

Fig. 8. Time-of-flight profile as a function of trapping time at V_{ac} = 118 V_{rms} (q_z = 0.582); U_{dc} = 15 V (a_z = −0.104); $\Omega/2\pi$ = 1 MHz at a neutral nitrogen pressure of $p(N_2) = 2.8 \times 10^{-8}$ mbar.

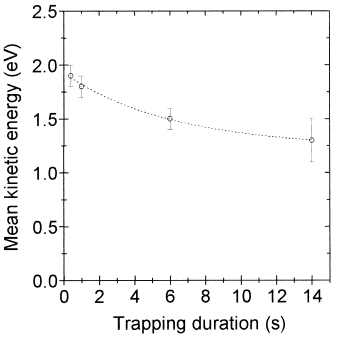

Fig. 10. Variation of the mean kinetic energy as function of trapping duration.

9). For this example, the increase of the evolution time leads to a slow decrease of the average kinetic energy (in the laboratory frame) from 1.9 to 1.3 eV. This evolution of the kinetic energy versus time is shown in Fig. 10.

The reported observations depend on the storage

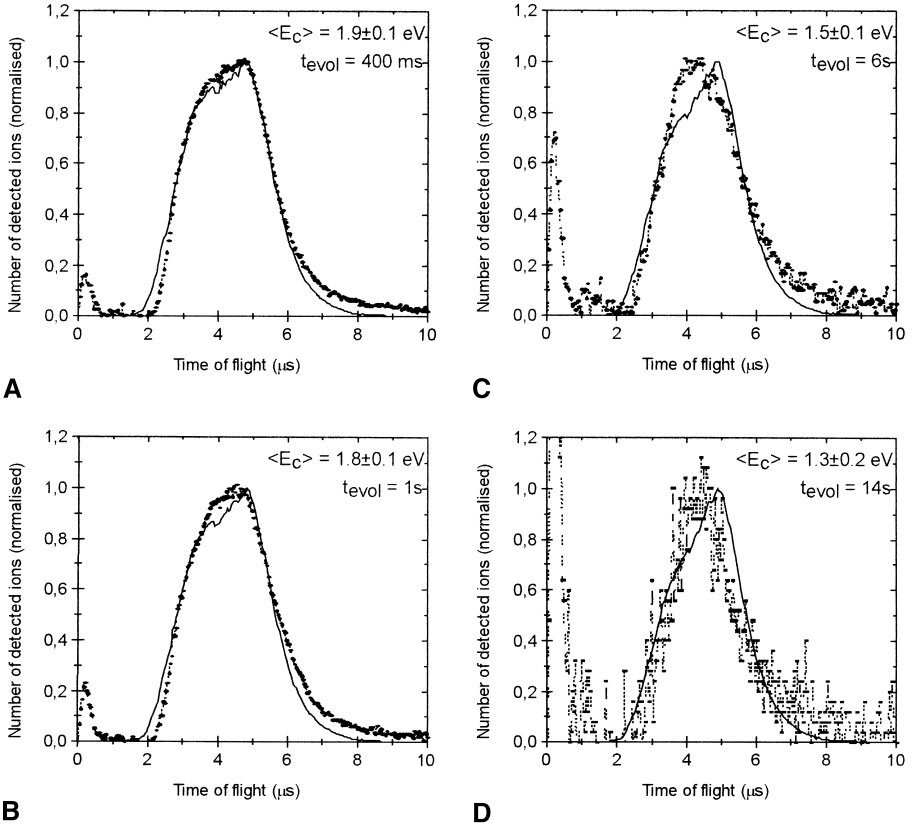

Fig. 9. Adjustment of the experimental (-●-●-●-) TOF profiles with the simulated (——) profiles at V_{ac} = 118 V_{rms} (q_z = 0.582); U_{dc} = 15 V (a_z = −0.104); $\Omega/2\pi$ = 1 MHz; V_{res} = 4 V.

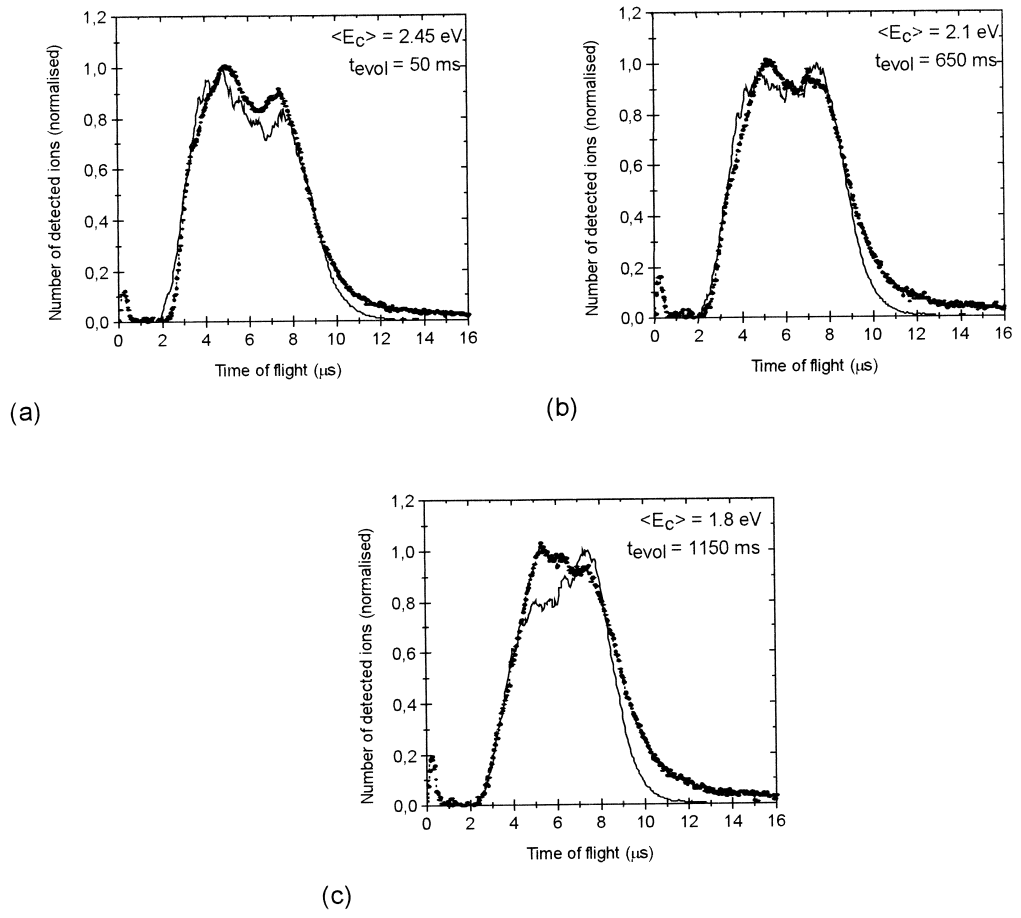

Fig. 11. Adjustment of the experimental (-●-●-●-) TOF profiles with the simulated (——) profiles at $V_{ac} = 113\ V_{rms}$ ($q_z = 0.558$); $U_{dc} = 3$ V ($a_z = -0.021$); $\Omega/2\pi = 1$ MHz; $V_{res} = 4$ V.

conditions (working point and pressure) (Fig. 11). Comparing Figs. 8 and 10, we could observe that for the latter working point the kinetic energy is higher for a storage time inferior to 1 s. Actually for these measurements, realised at higher pressure [$p(N_2) = 7.5\ 10^{-8}$ mbar], we have observed a very fast cooling process (from 2.4 to 1.8 eV for a trapping time increase of 1.1 s) accompanied by a different transformation of the experimental profile. In this case, ions were "transported" in the stability diagram. In fact, ions were created in a N_2^+-free region at $\Omega/2\pi = 1$ MHz, $V_{ac} = 113\ V_{rms}$, $U_{dc,crea} = 13$ V, they were then moved to a different working point ($V_{ac} = 113\ V_{rms}$, $U_{dc} = 3$ V). For longer storage times, it became very difficult to adjust the experimental signal with a simulated profile in a satisfactory way. This could be due to the loss of the faster ions caused by collisions, which can no longer be neglected. On this time scale, the fast evaporative cooling does not allow us to assume a Gaussian shape for the ion distributions anymore.

4. Conclusion

In this article, we have presented the results for kinetic energy measurements of an ion cloud with a versatile method. We have observed dependence of the kinetic energy of the ions on different parameters.

An important conclusion of these measurements is the fact that increasing the rf frequency will not necessarily lead to an increase in the kinetic energy as has already been observed in [11]. In our case, the energy is limited by evaporative cooling to almost 2.5 eV, essentially due to elastic collisions with heavier particles from the neutral parent gas [20]. This value can be confirmed by the almost complete absence of the endothermic charge-exchange process between N^+ and N_2, (the major neutral gas); the N^+ ion cloud does not attain the necessary threshold value for charge exchange [21]. The transformation of the shape of the ion cloud caused by evaporative cooling can also be demonstrated by the fact that the anisotropy coefficient used for the energy calibration was always about 1 in the case of the 1 MHz radiofrequency, while it could be close to 0.8 or 0.9 and even be as low as 0.6 for $\Omega/2\pi = 1.5$ MHz.

In conclusion, the presented TOF method by interruption of the confinement voltage does not perturb the ion cloud and its energetic properties. With the help of a model simulation, it can give robust estimations of the ion kinetic energy.

References

[1] R.E. March, J.F.J. Todd, CRC Series Modern Mass Spectrometry, CRC, Boca Raton, 1995.
[2] R.C. Thompson, Adv. Atom. Molec. Opt. Phys. 31 (1993) 63.
[3] H.G. Dehmelt, Adv. Atomic Molecular Phys. 3 (1967) 53.
[4] (a) F. Vedel, J. Andre, M. Vedel, G. Brincourt, Phys. Rev. A 27 (1983) 2321; (b) F. Vedel, J. Andre, ibid. 29 (1984) 2098.
[5] R. Iffländer, G. Werth, Metrologia 13 (1977) 167.
[6] F.L. Walls, T.S. Stein, Phys. Rev. Lett. 31 (1973) 975.
[7] M. Vedel, M. Knoop, D. Lunney, I. Rebatel, F. Vedel, Phys. Rev. A 51 (1995) 2294.
[8] M.D.N. Lunney, F. Buchinger, R.B. Moore, J. Mod. Opt. 39 (1992) 349.
[9] R.J. Champeau, A. Crubellier, J.O. Gaardsted, D. Marescaux, D. Pavolini, J. Phys. B 27 (1994) 905.
[10] E.R. Mosburg, M. Vedel, Y. Zerega, F. Vedel, J. Andre, Int. J. Mass Spectrom. Ion Processes 77 (1987) 1.
[11] F. Vedel, M. Vedel, J. Mod. Opt. 39 (1992) 431.
[12] F. Vedel, M. Vedel, R.E. March, Int. J. Mass Spectrom. Ion Processes 99 (1990) 125.
[13] J. Rocher, M. Vedel, F. Vedel, Int. J. Mass Spectrom. Ion Processes 181 (1998) 173.
[14] F. Vedel, M. Vedel, Phys. Rev. A 41 (1990) 2348.
[15] R. Alheit, S. Kleineidam, F. Vedel, M. Vedel, G. Werth, Int. J. Mass Spectrom. Ion Processes 154 (1996) 155.
[16] M. Vedel, J. Rocher, M. Knoop, F. Vedel, Appl. Phys. B 66 (1998) 191.
[17] F. Vedel, Int. J. Mass Spectrom. Ion Processes 106 (1991) 33, and references therein.
[18] H. Schaaf, U. Schmeling, G. Werth, Appl. Phys. 25 (1981) 249.
[19] A. Münch, M. Berkler, C. Gerz, D. Wilsdorf, G. Werth, Phys. Rev. A 35 (1987) 4147.
[20] M. Vedel, J. Andre, S. Chaillat-Negrel, F. Vedel, J. Phys. (France) 42 (1981) 541.
[21] (a) P.B. Armentrout, T. Baer, J. Phys. Chem. 100 (1994) 12877; (b) S. Mark, D. Gerlich, Chem. Phys. 209 (1996) 235.